Analytical analysis of the resonance response of subwavelength nanoscale cylindrical apertures in metal at near ultraviolet, optical, and near infrared frequencies

Eli Lansey,[1,*] Nafiseh Pishbin,[2] Jonah N. Gollub,[3] and David T. Crouse[4]

[1] *Department of Physics, Graduate Center and City College of the City University of New York*

[2] *Department of Electrical Engineering, Graduate Center and City College of the City University of New York*

[3] *Phoebus Optoelectronics*

[4] *Department of Electrical Engineering, City College of the City University of New York*

[*] *Corresponding author: elansey@gc.cuny.edu*

In this paper we analytically study the resonance response of cylindrical subwavelength apertures embedded in metal films at near UV, optical, and near IR frequencies. This analysis is concise, and allows accurate and intuitive prediction of both propagating and evanescent modes, which are key contributors to enhanced optical transmission through thin metal films. In this approach we do not analyze the detailed behavior of the fields inside the metal walls, but still obtain the effects of the implicit buildup of charges within those walls. We calculate the modal dispersion relation, cutoff dependence on cylinder radius, and waveguide attenuation for a cylindrical aperture embedded in metal. We support our findings with finite element simulations and find strong agreement with our theory.

OCIS codes: 160.3918, 160.4236, 310.6628, 350.4238.

1. Introduction

Enhanced optical transmission (EOT) was first experimentally observed by T.W. Ebbesen in 1998 and has since been shown to have a wide range of applications, including light concentration and trapping [1–13]. Past work has highlighted that the excitation of fields inside gratings and apertures can lead to exceptionally high light concentration within the confined spaces of 1D cavities or gratings, as well as enhanced transmission through the gratings [14–16].

A full and accurate analysis of EOT using finite element or finite difference time domain simulations requires significant computer resources and long calculation times. Therefore, a quick method to determine the modal response of cavity modes is of great utility for the design of optical structures. Thus, there has since been a major effort to describe EOT theoretically.

There is a large body of work analyzing these structures assuming the metal is a perfect electric conductor (PEC) [17–19]. These models have the benefit of being largely analytical in nature. However, these approaches are poor models for optical EOT, as metals at optical frequencies display large variation in their dielectric functions, and are far from perfect conductors.

A recent thorough survey of approaches towards modeling EOT can be found in reference [20]. In that review, many theoretical models are compared via the heavily utilized, semi-analytic coupled-wave (CW) analysis. This CW approach yields results with varying degrees of agreement with simulation and experiment, but they are all, ultimately, numerical solutions. That is, trends and dependencies must be empirically deduced from the results.

Thus, a first-principles approach to describe EOT is desirable. One recent approach treats the cavity-metal structure at optical frequencies as a dielectric core-cladding fiber optic (FO) analogue and uses established techniques to numerically solve for the resulting modal dispersion curves [21–23]. The calculated modes are then analogous to propagating fiber optic modes, with TE, TM, or hybrid TE/TM-type waveguide modes.

The FO approach has the benefit of appealing to the vast body of work involving fiber optics, but it has a few notable limitations. First, it assumes the primary cause of EOT is via the excitation of propagating waveguide modes (WM). While this is a valid approximation for optically thick films, in thin films, however, the decay length of evanescent waveguide modes can be many multiples of the film thickness and would thus also contribute to EOT. Secondly, it numerically requires using a lossless Drude model for the metal dielectric, which does not adequately match the actual physical properties of most metals at optical frequencies. Furthermore, while this approach can be used for cylindrical apertures, it is difficult to generalize for other geometries. Finally, the dispersion curves must always be calculated numerically using this method, and is thus limited in a similar manner as the CW approaches.

Nevertheless, dispersion analysis is a powerful approach for determining the waveguide cavity modes that can be excited within a particular aperture. In this paper we present an analytical theory for calculating the modal dispersion curves of cylindrical apertures in real metals. We frame our approach using waveguide analysis with an approximate "skin depth boundary condition" (SDBC) at the cavity walls. We use this approximation to find an equivalent effective PEC cavity and its modal dispersion properties.

This analysis carries all the benefits of dispersion analysis as discussed in [23], for example, with the added benefit of determining the evanescent modes and including real metal parameters. This approach describes the fundamental behavior of WMs at optical frequencies using approximate boundary conditions. Unlike many other approaches, this theoretical model directly predicts the dispersion curve, and its dependence on aperture dimensions and metal parameters, without needing to rely on interpretation of numerical solutions.

2. Waveguide solutions

Here we discuss a cylindrical aperture of radius a, filled with dielectric ϵ embedded in a metal film. We neglect any magnetic effects, taking $\mu = 1$ for all materials, see Fig. 1. Waveguide cavity modes are solutions ψ_{mn} to the 2D wave equation,

$$\left[\nabla^2 + \left(\epsilon\kappa_0^2 - k_z^2\right)\right]\psi_{mn} = 0, \tag{1}$$

where $\kappa_0 \equiv \omega/c$, and k_z is the propagation constant along the length of the aperture [25]. The solutions to this equation in cylindrical coordinates take the form,

$$\psi_{mn}(r,\phi) = e^{im\phi} J_m\left(\beta_{mn} r\right), \tag{2}$$

where the z-component of the electric field is,

$$E_z(r,\phi,z) = \psi e^{ik_z z}. \tag{3}$$

Here, J_m is the m-th Bessel function of the first kind, and the value of m and the radial wavevector β_{mn} is determined from boundary conditions. We only show explicit calculations for TM modes in this paper, but the analysis applies to TE modes as well.

2.A. Approximate boundary condition

In our analysis we use an approximate boundary condition to find the values of m and β_{mn}. Since metals at optical frequencies do not have infinite conductance, we relax the requirement that the fields just inside the metal wall drop to zero. That is, for a real metal, charges build up inside the surface of the walls of the aperture over some skin depth, δ. Although these

charge distributions need not be cylindrically symmetric, we still require 2π periodicity in the ϕ direction, so m must take an integer value.

Although the metallic skin depths at optical frequencies can be large, beyond that depth we expect metals to behave like perfect conductors, i.e. the fields drop rapidly to zero. When δ is significantly smaller than the characteristic aperture dimension, a, typically on the order of the wavelength λ, this allows significant simplification of the resulting equations. Fig. 2 shows the variation of the ratio δ/λ for a few metals over a range of frequencies. The small value of this ratio motivates our approximation.

Our approach here is to find an effective cavity which accurately captures the properties of the aperture as well as the effect of the real metal walls. It has already been shown with stacked photonic crystal nanocavities that resonance properties of a complicated structure can be accurately described by determining an effective resonant cavity with PEC walls [24]. Here, too, we find an effective PEC cavity using the skin depth as the limiting length scale.

The fields inside the metal walls can be written in terms of Hankel functions of the first kind [21], which decay extremely rapidly. Thus, the majority of the fields in the metal are constrained within a very small region close to the surface of the aperture. We make the reasonable assumption that upon reaching one skin depth into the metal we have accounted for the contribution of the fields within the metal, and beyond that point it is effectively a PEC. This argument is supported by the strong agreement of this model to simulated results (see Fig. 3).

Then, for a cylindrical aperture of radius a centered at the origin, we can apply the perfect electric conductor boundary conditions:

$$\hat{n} \times \vec{E} = 0, \tag{4a}$$

$$\hat{n} \cdot \vec{H} = 0, \tag{4b}$$

where $\hat{n}$ is a unit normal to the cavity wall, at a radial distance $r = a + \delta$ rather than at the cavity walls ($r = a$).

It is important to highlight that this analysis does not describe the complete details of the fields' behavior within the metal. This is different than many other approaches discussed in the introduction that do, in fact, describe the fields in the metal explicitly. Instead we consider only the overall effect that the imperfect conductor has on the behavior of the fields within the cavity itself. This simplification allows us to avoid relying on numerical techniques to determine these effects.

3. Dispersion analysis

Using conservation of energy, or by substituting Eq. (2) into Eq. (1), we get the dispersion relation,

$$\epsilon\frac{\omega^2}{c^2} = k_z^2 + \beta^2, \tag{5}$$

where ω is the angular frequency, c is the speed of light, and β is found by evaluating $J_m\left[\beta(a+\delta)\right] = 0$. Applying these conditions gives

$$\beta = \left(\frac{1}{1+\xi}\right)\beta_0 \tag{6}$$

where $\beta_0 \equiv \chi_{mn}/a$, with χ_{mn} being the nth root of the mth Bessel function, and $\xi \equiv \delta/a$. Note, that for a perfect conductor $\delta \to 0$ so $\xi \to 0$, and we recover the well-known waveguide modes β_0 [25]. As the relative length of the skin depth increases (i.e. the metal becomes increasingly less PEC-like), ξ increases, and the magnitude of the transverse wavevector decreases. This, in turn, shifts the dispersion curve toward lower frequencies (see Fig. 3, inset).

Equation 5 has the benefit of solving for all possible modes, both propagating (real k_z) and evanescent (imaginary k_z). It is well known that near-field evanescent fields can contribute significantly to the ability of structures to couple to incident light as well as transmitted waves [20, 26]. Furthermore, as discussed earlier, the decay length can be many multiples of film thickness in thin films, whereby evanescent modes directly contribute to EOT. Hence, solving for all modes, both propagating and evanescent, produces a more complete picture of the resonance behavior of these nanoresonator apertures.

3.A. Sample comparison with simulation

The skin depth at various frequencies can be calculated using

$$\delta(\omega) = \frac{c}{\omega\kappa(\omega)}, \tag{7}$$

where

$$\kappa(\omega) = \sqrt{\frac{1}{2}\sqrt{\Im\left[\epsilon_m(\omega)\right]^2 + \Re\left[\epsilon_m(\omega)\right]^2} - \frac{1}{2}\Re\left[\epsilon_m(\omega)\right]}, \tag{8}$$

is the imaginary part of the index of refraction of the metal [27], and where the value of the dielectric constant, ϵ_m, of the metal can be found experimentally or through use of a Drude model,

$$\epsilon_m(\omega) = 1 - \frac{\omega_p^2}{\omega(\omega - i\omega_\tau)}, \tag{9}$$

where ω_p is the plasma frequency and ω_τ is the collision frequency [28].

Figure 3 shows a number of dispersion curves for silver apertures with $a = 190\,\text{nm}$, $\omega_p = 1.37 \times 10^{16}\,\text{s}^{-1}$ and $\omega_\tau = 7.29 \times 10^{13}\,\text{s}^{-1}$, calculated using this method, along with finite element full-wave eigenmode simulations of the same structure. As the figure shows, there is strong agreement between the theoretical prediction and the simulation results. The inset shows the curves predicted by this model as well as the curves using a PEC boundary condition. The shift to lower frequencies seen here is due to the effectively larger cavity.

4. Cutoff dependence

Using the cutoff condition, $k_z = 0$, we can solve Eq. (5) for the cutoff frequency, ω_{cutoff}, of a mode in terms of the radius, a, of an aperture which supports it. Practically, due to the frequency dependance of δ, it's easier to directly calculate the radius

$$a = \frac{c}{\omega_{\text{cutoff}}} \frac{\chi_{mn}}{\sqrt{\epsilon}} - \delta\left(\omega_{\text{cutoff}}\right) \tag{10}$$

in terms of ω_{cutoff}. Note how apertures with smaller radii (by a subtractive factor of δ) permit higher frequency resonances as compared to the perfect electric conductor condition. Here, too, when $\delta \to 0$ as in a PEC we recover the well-known cutoff result. Fig. 4 shows a plot of f_{cutoff} as a function of the radius a for a few TM modes in silver. Note that for a given radius the cutoff frequency is lower using this model, again due to the effectively larger cavity size.

The general trend of these results have been known empirically for some time, from experimental and numerical methods [12]. Here, though, we predict these properties in an intuitive analytical form. Therefore, we view those established results as a confirmation of the theoretical approach developed here.

5. Effect on fields and induced charges and currents

Using Eq. (2) with Eq. (6) allows us to calculate the field profiles within the apertures. Fig. 5 shows some calculated fields for a few TM modes for $\xi = 0.15$. Note that these fields are only plotted within the cavity, and not into the cavity walls, as we have not analyzed the detailed behavior of the fields within the metal, only the net effect it has on the cavity response. Additionally, note that the fields do not drop to zero at the cavity walls as they do for a perfect conductor.

For $\xi \ll 1$, we can expand Eq. (2) in powers of ξ. Keeping through quadratic terms, we have

$$\psi(r,\phi) = \{J_m\left(\beta_0 r\right) - \frac{1}{2}\xi(\xi-2)\beta_0 r J_{m+1}\left(\beta_0 r\right) + \frac{1}{2}\xi\left[m(m\xi+\xi-2) - \xi\beta_0^2 r^2\right] J_m\left(\beta_0 r\right)\} e^{im\phi}. \tag{11}$$

This corresponds to the perfect electric conductor field $J_m(\beta_0 r)$ plus a correction due to the additional buildup of charges in the metal.

Fig. 6 shows a plot of ψ for $m = 0$, $n = 2$ and $\xi = 0.1$. If the dielectric of the metal is calculated using Eq. (9) with $a = 190\,\text{nm}$, this value of ξ corresponds to $f = 611\,\text{thz}$. The thin line is the PEC field component of Eq. (11), with the dashed line being the correction due to our method. The thick black line corresponds to the total field behavior. We have additionally plotted the decay of the fields into the metal wall. Note that the dominant contribution to total field strength is from the portion of the field concentrated within the cavity, with only small portions of the field penetrating into the metal.

Eq. (11) shows that for good conductors (i.e. small ξ) there is no shift in the resonance of the cavity for the lowest order modes, while there is a change in the overall field behavior accounting for the buildup of additional surface charges. For larger ξ or higher order modes, however, it is necessary to use the complete expressions Eqs. (2) and (6) to calculate the dispersion relation. Additionally, although ξ varies as a function of frequency, if there is minimal variation of this value over the frequency region of interest, it is straightforward to calculate the shift in resonance using Eq. (6).

Furthermore, note that at the metal surface, $r = a$, there is a nonzero E_z field equal to

$$E_z = -\frac{1}{2}\xi(\xi - 2)\chi_{mn} J_{m+1}[\chi_{mn}] e^{im\phi}. \tag{12}$$

This correction can be thought of as the contribution to the field from an effective distribution of surface plasmon charges, σ_{sp}, on the surface of the metal. This is in addition to the surface charges, σ_{pec}, which arrange themselves on a perfect conductor to counterbalance the incident field. Then, the total surface charge on the metal is

$$\sigma = \sigma_{\text{pec}} + \sigma_{\text{sp}}. \tag{13}$$

We find the value of σ using the continuity expressions

$$\hat{n} \cdot (\vec{D}_2 - \vec{D}_1) = 4\pi\sigma \tag{14}$$

resulting from Gauss's law [25], where $\hat{n}$ is a unit normal from region 1 to region 2. Requiring the field inside the metal ($\vec{D}_2$) to drop to zero, we get

$$\sigma_{\text{pec}} = \frac{i\epsilon k_z}{4\pi}\frac{\beta_0}{\beta^2} J_{m+1}[\chi_{mn}] e^{im\phi}, \tag{15a}$$

$$\sigma_{\text{sp}} = -\frac{1}{2}\xi^2\left(\chi_{mn}^2 - m^2\right)\sigma_{\text{pec}}. \tag{15b}$$

where the value of k_z is determined by Eq. (5) and β by Eq. (6). These expressions result

from first operating on Eq. (2), and then expanding in powers of ξ. Note that $\chi_{mn}^2 > m^2$, so this additional effective surface charge distribution is always of opposite sign to the perfect conductor distribution.

We can likewise break the induced effective surface current,

$$\vec{J} = \vec{J}_{\rm pec} + \vec{J}_{\rm sp}, \tag{16}$$

into the current, $\vec{J}_{\rm pec}$, present in a perfect conductor and the surface plasmon current $\vec{J}_{\rm sp}$. Using the continuity expressions,

$$\hat{n} \times (\vec{B}_2 - \vec{B}_1) = \frac{4\pi}{c}\vec{J}, \tag{17}$$

requiring the field inside the metal ($\vec{B}_2$) to drop to zero, we get currents

$$\vec{J}_{\rm pec} = \hat{z}\,\frac{ic\epsilon\kappa_0}{4\pi}\frac{\beta_0}{\beta^2}J_{m+1}[\chi_{mn}]e^{im\phi}, \tag{18a}$$

$$\vec{J}_{\rm sp} = -\frac{1}{2}\xi^2\left(\chi_{mn}^2 - m^2\right)\vec{J}_{\rm pec}, \tag{18b}$$

traveling upwards and downwards. Here the additional induced current travels in the opposite direction to the current induced in a perfect conductor. This decrease in current is due to the resistive losses in the metal.

6. Attenuation

We can also use these results to calculate, α, the time-averaged fractional power lost per unit length of the cavity. The time-average power absorbed per unit length is [25]

$$P_{\rm abs} = \frac{a\omega\delta}{4}\left|H_\phi\right|^2, \tag{19}$$

while the time average power transmitted per unit length, $P_{\rm trans}$, is found by taking the $\hat{z}$ component of the real part of the Poynting vector, integrated over the area of the aperture. The ratio

$$\alpha \equiv \frac{P_{\rm abs}}{P_{\rm trans}} = \frac{2\xi}{(1+4\xi)}\frac{\epsilon\kappa_0^2}{k_z} \tag{20}$$

is the power lost per unit length in propagating modes, normalized with respect to the amount of power flowing down the cavity. Here we have again kept through quadratic terms in ξ. Thus, the power, P, decays as a function of z by

$$P(z) = P_0 e^{-\alpha z}, \tag{21}$$

where P_0 is the incident power.

Figure 7 shows the variation of α as a function of frequency. After the initial drop in loss above the cutoff, α increases with frequency due to larger portions of the field penetrating into the metal. Note that this expression only holds above the cutoff frequency; below cutoff the attenuation is given by the imaginary part of k_z.

Furthermore, as seen in Fig. 7, for an aperture of a particular radius there is a frequency at which the loss is minimized. This frequency can be found by finding the roots of

$$\frac{\epsilon\kappa_0^2}{\beta_0^2} = \frac{2\xi(1+5\xi) + (1+2\xi+4\xi^2)\,\omega\xi'}{\xi(1+7\xi) + (1+3\xi+3\xi^2)\,\omega\xi'}, \tag{22}$$

in terms of ω, where $\xi' \equiv d\xi/d\omega$. This solution will depend on the explicit form of $\xi(\omega)$ for a given metal, as well as the particular radius of interest.

It is worthwhile to note that there is no minimum to α with respect to the aperture radius. For larger radii, α tends towards zero, as the propagating energy is proportional to a^2, while, for a particular frequency, the skin depth is fixed. Thus, the relative amount of loss decreases with increasing radius.

7. Summary and conclusion

We have presented a new analytical model for waveguide resonance in real metals, which is a first step in developing a general model for EOT. Unlike other methods, this simple approach allows direct analytic predictions of various resonance properties, without needing to rely on CW analyses or other numerical techniques. We have shown, through illustrative examples with silver, strong agreement between the theory and simulated results, and some predictions of this model are confirmed by long-known experiments, as well.

Although the model was applied to apertures in silver, another major advantage of this approach is that the analytical form of the field response of all metals and cylindrical apertures is the same. The differences between various metals and frequencies are determined only by the value of ξ. This allows easy and accurate prediction of waveguide resonance properties, without relying on complicated or time-consuming numerical calculations and simulation. Furthermore, it is easy to measure values of metal dielectrics and calculate values for ξ to incorporate in this analysis, and not rely on a Drude model.

Additionally, these results can be used as part of a larger theoretical framework to find the complete resonance and transmission response of apertures embedded in metallic films of finite thickness. For example, additional restrictions can be placed on k_z transforming the waveguide into a resonant cavity. These restrictions would arise from boundary conditions across the aperture openings. For example, a transmission/reflection matrix method can be used to determine these restrictions, and, together with the methods described in this paper,

can be used to find the resonance frequencies of the cavity along with quality-factor of the resonances. A detailed analysis of these applications, however, is beyond the scope of this paper.

This approach can also be generalized to apertures of arbitrary shape. The general solutions to the wave equation Eq. (1) determine the functional form of the cavity modes, while the dispersion relation of Eq. (5) is generalized to

$$\epsilon \frac{\omega^2}{c^2} = k_z^2 + \gamma^2, \tag{23}$$

where γ, the generalized transverse wavevector, replaces the radial wavevector β. The value of γ is found by evaluating boundary conditions Eq. (4) at a distance δ into the cavity walls, see Fig. 8. For particular geometries, it is also possible to decouple TE and TM modes as we have here.

Of particular interest are rectangular waveguides which are difficult to solve using the aforementioned fiber-optic method [29, 30]. However, using the general approach of this paper yields a quick, analytic solution. The response of rectangular apertures is polarization dependant, and as such has many applications in polarimetry. Here too, a detailed analysis of this application is beyond the scope of this paper, nevertheless, the ability to accurately predict the resonance properties of subwavelength apertures is of great utility.

Acknowledgments

This material is based upon work supported by the DOD/DARPA SBIR PROGRAM under Contract No. W31P4Q-10-C-0074. The views, opinions, and/or findings contained in this article/presentation are those of the author/presenter and should not be interpreted as representing the official views or policies, either expressed or implied, of the Defense Advanced Research Projects Agency or the Department of Defense. It has been approved for public release, distribution unlimited.

References

1. T. W. Ebbesen, H. J. Lezec, H. F. Ghaemil, T. Thiol, and P. A. Wolff, "Extraordinary optical transmission through sub-wavelength hole arrays," Nature **391**, 667–669 (1998). EOT.
2. D. Zhou and R. Biswas, "Photonic crystal enhanced light-trapping in thin film solar cells," Journal of Applied Physics **103**, 093102 (2008).

3. M. Bayindir, B. Temelkuran, and E. Ozbay, "Photonic-crystal-based beam splitters," Applied Physics Letters **77**, 3902–3904 (2000).
4. M. Z. Tidrow and W. R. Dyer, "Infrared sensors for ballistic missile defense," Infrared Physics & Technology **42**, 333 – 336 (2001).
5. D. Kim, C. Warde, K. Vaccaro, and C. Woods, "Imaging multispectral polarimetric sensor: Single-pixel design, fabrication, and characterization," Appl. Opt. **42**, 3756–3764 (2003).
6. C. Genet and T. W. Ebbesen, "Light in tiny holes," Nature **445**, 39–46 (2007).
7. H. Cao, A. Agrawal, and A. Nahata, "Controlling the transmission resonance lineshape of a single subwavelength aperture," Opt. Express **13**, 763–769 (2005).
8. A. Degiron and T. Ebbesen, "Analysis of the transmission process through single apertures surrounded by periodic corrugations," Opt. Express **12**, 3694–3700 (2004).
9. H. Lochbihler and R. Depine, "Highly conducting wire gratings in the resonance region," Applied Optics **32**, 3459–3465 (1993).
10. J. A. Porto, F. J. García-Vidal, and J. B. Pendry, "Transmission resonances on metallic gratings with very narrow slits," Phys. Rev. Lett. **83**, 2845–2848 (1999).
11. Q. Cao and P. Lalanne, "Negative role of surface plasmons in the transmission of metallic gratings with very narrow slits," Phys. Rev. Lett. **88**, 057403 (2002).
12. F. J. García-Vidal and L. Martín-Moreno, "Transmission and focusing of light in one-dimensional periodically nanostructured metals," Phys. Rev. B **66**, 155412 (2002).
13. A. Barbara, P. Quémerais, E. Bustarret, and T. Lopez-Rios, "Optical transmission through subwavelength metallic gratings," Phys. Rev. B **66**, 161403 (2002).
14. D. Crouse, "Numerical modeling and electromagnetic resonant modes in complex grating structures and optoelectronic device applications," IEEE Transactions on Electron Devices **52**, 2365 – 2373 (2005).
15. D. Crouse, A. P. Hibbins, and M. J. Lockyear, "Tuning the polarization state of enhanced transmission in gratings," Applied Physics Letters **92**, 191105 (2008).

16. D. Crouse and P. Keshavareddy, "Polarization independent enhanced optical transmission in one-dimensional gratings and device applications," Opt. Express **15**, 1415–1427 (2007).
17. H. A. Bethe, "Theory of diffraction by small holes," Phys. Rev. **66**, 163–182 (1944).
18. R. Gordon, "Bethe's aperture theory for arrays," Phys. Rev. A **76**, 053806 (2007).
19. A. Y. Nikitin, D. Zueco, F. J. García-Vidal, and L. Martín-Moreno, "Electromagnetic wave transmission through a small hole in a perfect electric conductor of finite thickness," Phys. Rev. B **78**, 165429– (2008).
20. F. J. García-Vidal, L. Martín-Moreno, T. W. Ebbesen, and L. Kuipers, "Light passing through subwavelength apertures," Rev. Mod. Phys. **82**, 729–787 (2010).
21. L. Novotny and C. Hafner, "Light propagation in a cylindrical waveguide with a complex, metallic, dielectric function," Phys. Rev. E **50**, 4094–4106 (1994).
22. H. Shin, P. B. Catrysse, and S. Fan, "Effect of the plasmonic dispersion relation on the transmission properties of subwavelength cylindrical holes," Phys. Rev. B **72**, 085436 (2005).
23. P. B. Catrysse and S. Fan, "Propagating plasmonic mode in nanoscale apertures and its implications for extraordinary transmission," Journal of Nanophotonics **2**, 021790 (2008).
24. P. Lalanne, C. Sauvan, and J. Hugonin, "Photon confinement in photonic crystal nanocavities," Laser & Photonics Reviews **2**, 514–526 (2008).
25. J. Jackson, *Classical Electrodynamics* (John Wiley & Sons, Inc., 1975), 2nd ed.
26. H. Lezec and T. Thio, "Diffracted evanescent wave model for enhanced and suppressed optical transmission through subwavelength hole arrays," Opt. Express **12**, 3629–3651 (2004).
27. S. Kawata and V. M. Shalaev, eds., *Tip Enhancement* (Elsevier Science, 2007).
28. M. A. Ordal, R. J. Bell, J. R. W. Alexander, L. L. Long, and M. R. Querry, "Optical properties of fourteen metals in the infrared and far infrared: Al, co, cu, au, fe, pb, mo,

ni, pd, pt, ag, ti, v, and w." Appl. Opt. **24**, 4493–4499 (1985).

29. A. Sudbo, "Why are accurate computations of mode fields in rectangular dielectric waveguides difficult?" Lightwave Technology, Journal of **10**, 418 –419 (1992).

30. G. R. Hadley, "High-accuracy finite-difference equations for dielectric waveguide analysis ii:dielectric corners," J. Lightwave Technol. **20**, 1219 (2002).

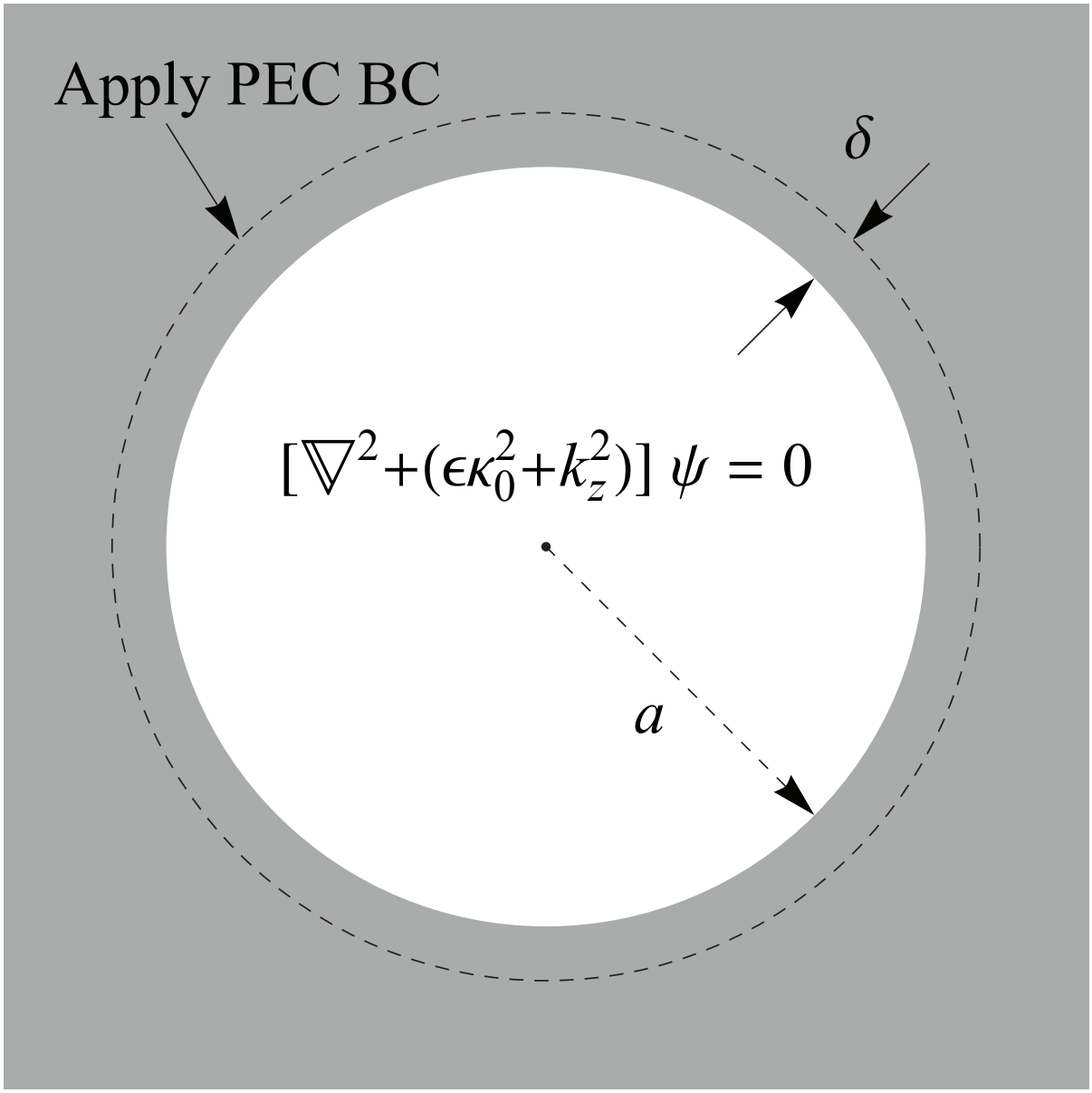

Fig. 1. Schematic of cylinder waveguide geometry and solution strategy. The gray region represents the metal, and the white region is the dielectric-filled aperture.

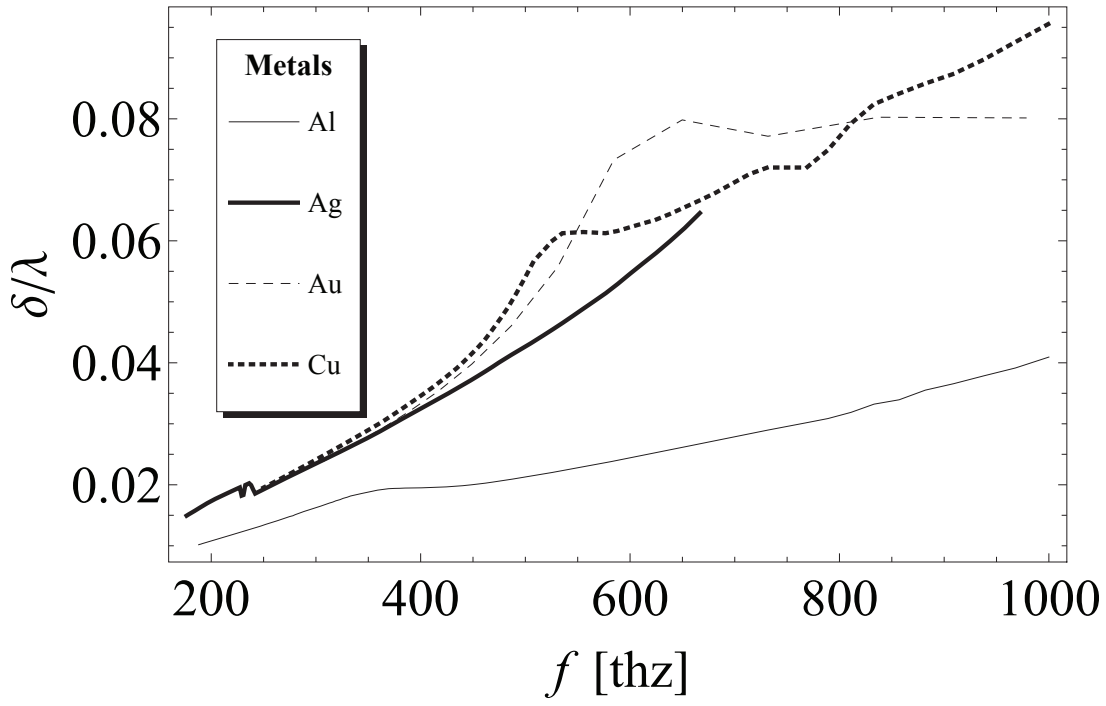

Fig. 2. The ratio of δ/λ for a few metals over a range of frequencies.

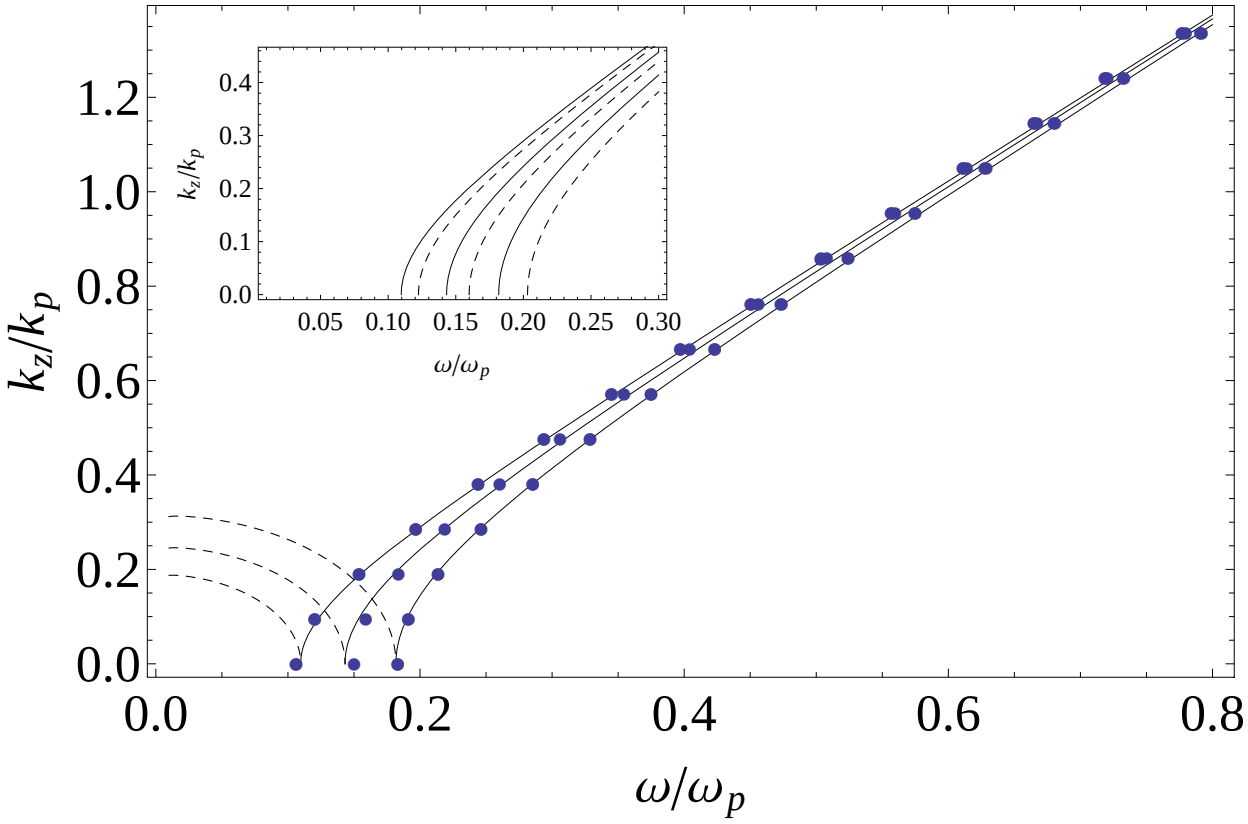

Fig. 3. The real (solid) and imaginary (dashed) dispersion curves calculated and simulated (points) for cylindrical apertures of radius $a = 190\,\text{nm}$ filled with a dielectric $\epsilon = 3$ embedded in Drude silver. Here $k_p \equiv \omega_p/c$. Inset shows results using this method (solid) compared to PEC modal dispersion (dashed).

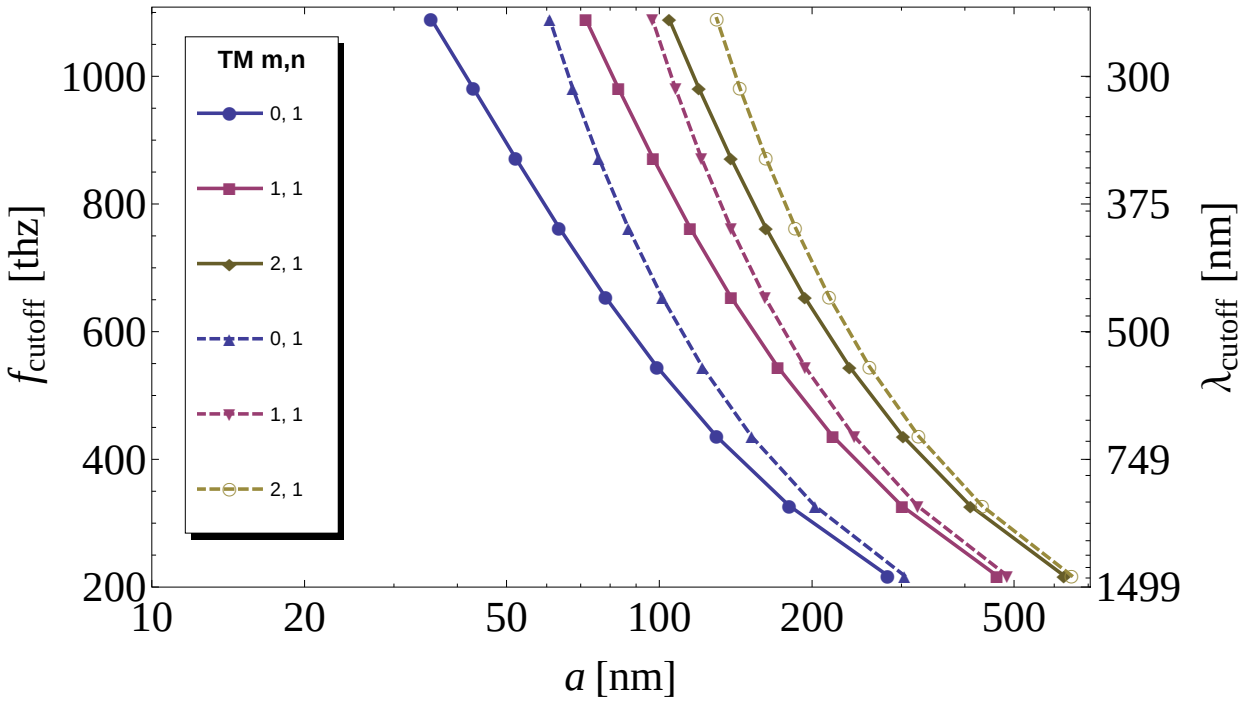

Fig. 4. (Color online) The TM cutoff frequency f_{cutoff} as a function of the radius a for a few modes $m = 0, 1, 2$ and $n = 1$ in silver. The solid lines are calculated using the method described in this paper, the dashed lines are curves using for a perfect conductor.

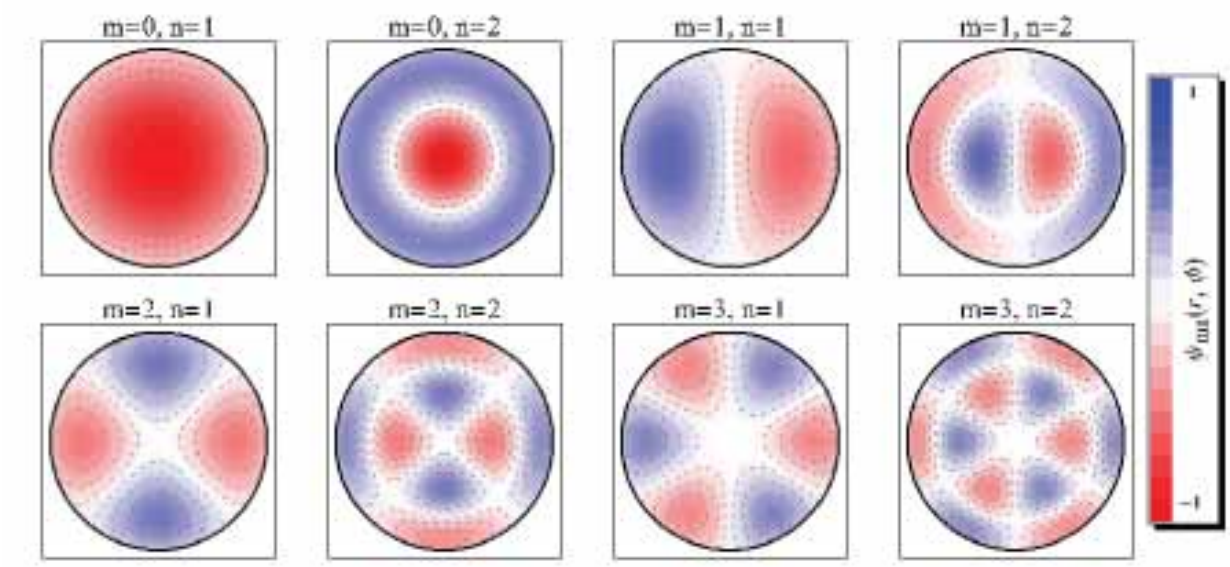

Fig. 5. (Color online) Calculated TM ψ fields in silver with $\xi = 0.15$.

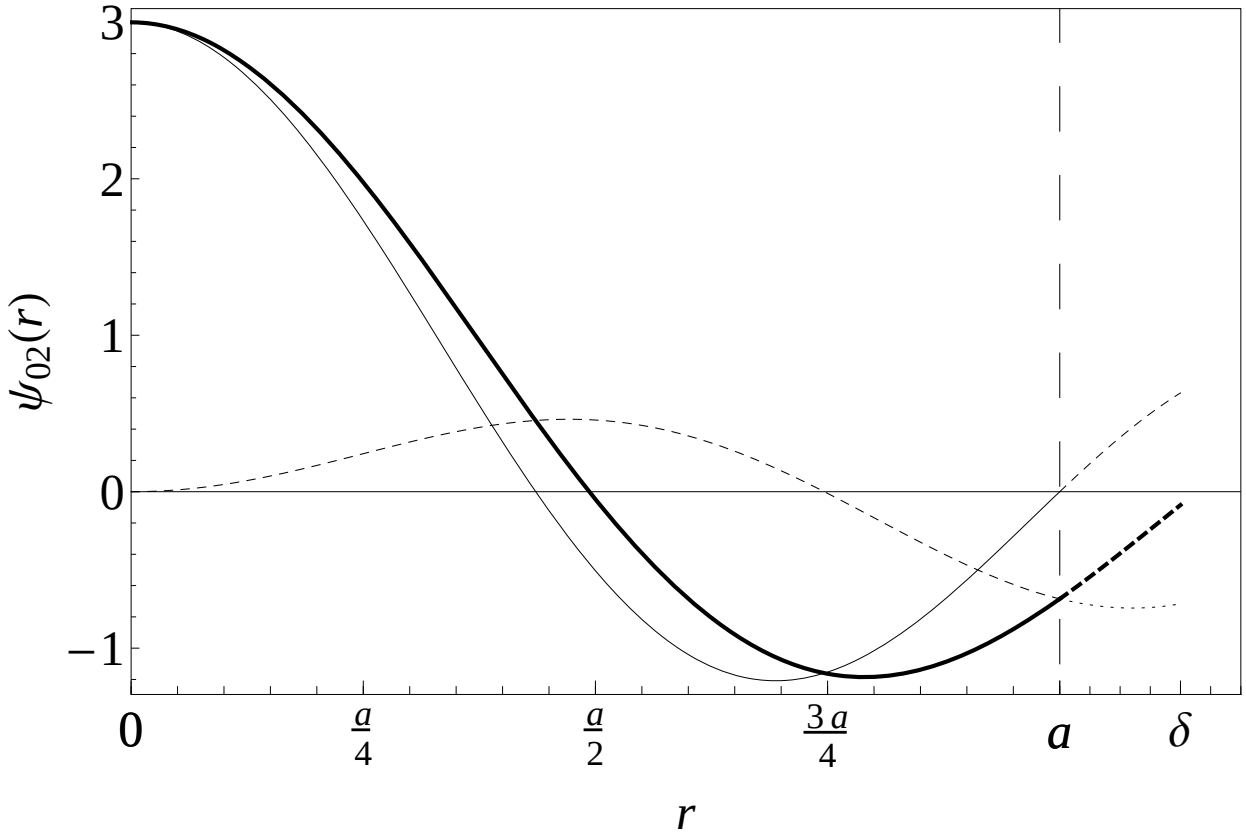

Fig. 6. The radial field dependance of ψ for a TM mode using Eq. (11) for $m = 0$, $n = 2$, and $\xi = 0.1$. The thin line is the perfect conductor waveguide mode, the dashed line is the contribution due to additional charges in the metal, and the thick line is the superposition of the two. The vertical dashed line indicates the position of the cavity walls. The rapid decay of the field inside the cavity walls is also plotted.

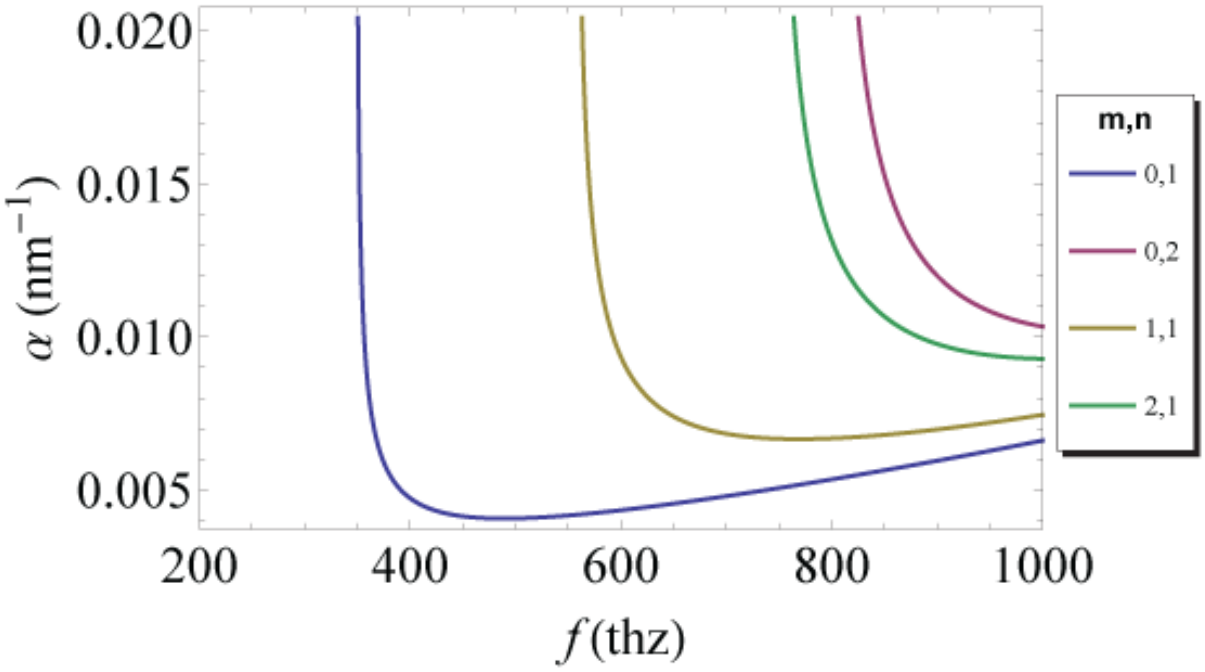

Fig. 7. (Color online) The fractional power loss α per unit length of a cylindrical apertures of radius $a = 190\,\mathrm{nm}$ filled with a dielectric $\epsilon = 3$ embedded in Drude silver. The loss is plotted for a few resonant modes.

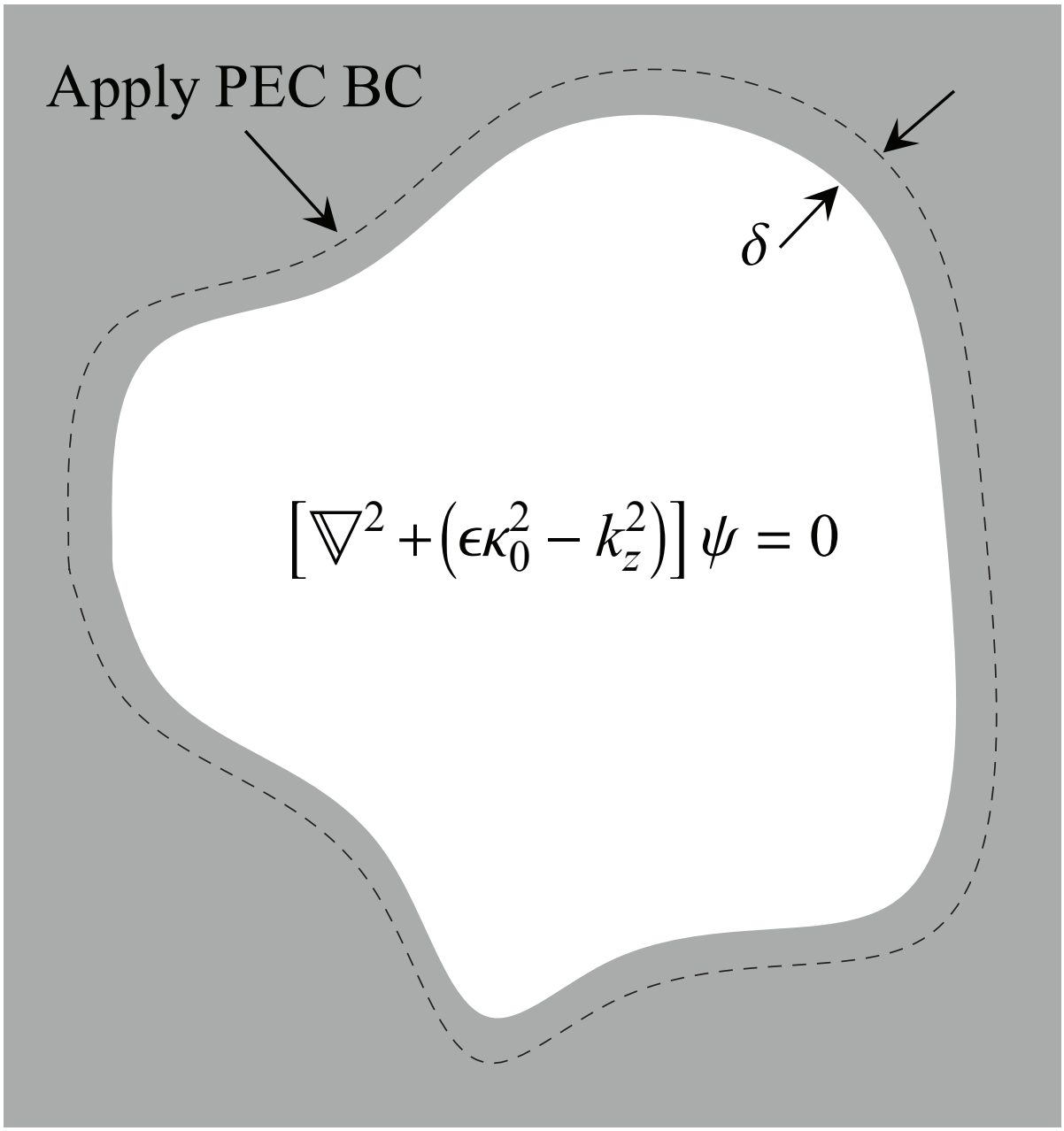

Fig. 8. Schematic of an arbitrarily-shaped cavity and solution strategy. The gray region represents the metal, and the white region is the dielectric-filled cavity.